Journal of Loss Prevention in the Process Industries 78 (2022) 104815

Contents lists available at ScienceDirect

Journal of Loss Prevention in the Process Industries

journal homepage: www.elsevier.com/locate/jlp

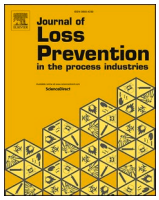

On the flammable behavior of non-traditional dusts: Dimensionless numbers evaluation for nylon 6,6 short fibers

Maria Portarapillo [a,*], Enrico Danzi [b], Gianluca Guida [a], Giuseppina Luciani [a], Luca Marmo [b], Roberto Sanchirico [c], Almerinda Di Benedetto [a]

[a] Department of Chemical, Materials and Production Engineering, University of Naples Federico II, P.le V. Tecchio 80, 80125, Naples, Italy
[b] Department of Applied Science and Technology-Politecnico di Torino, C.so Duca degli Abruzzi 21, 10129, Torino, Italy
[c] Istituto di Scienze e Tecnologie per l'Energia e la Mobilità Sostenibili (STEMS-CNR), P.le V. Tecchio 80, 80125, Napoli, Italy

ARTICLE INFO

Keywords:
Process safety
Dust flammability
TG/DSC analysis
Oxygen diffusion

ABSTRACT

Safety parameters assessment is not sufficient to fully understand the flammable and explosive behaviour of a combustible dust and correctly manage potential risk. A correct evaluation requires the identification of flame propagation path as well as the limiting step controlling fire propagation, through evaluation of dimensionless numbers (Biot, Damköhler, Thiele, Sherwood, Thiele modulus numbers). Herein, these aspects were investigated for non-traditional dusts, made of nylon 6,6 short fibers. To this purpose, flammability parameters including minimum ignition energy (MIE), the maximum pressure of explosion and the deflagration index were assessed and combined with results of extensive physical-chemical characterization, by means of several techniques (TGA/DSC, FTIR, XRD). In particular, thermogravimetric analysis highlighted the presence of homogeneous and heterogeneous phase phenomena activated at different temperatures and heating rates. The homogeneous phase processes are controlled by the pyrolysis process strictly dependent on the dust size and its decomposition kinetics. The most flammable sample is characterized by smaller dimensions and a fast decomposition kinetics at low temperature. Heterogeneous flame propagation is controlled by the intrinsic heterogeneous reaction. The most reactive sample is characterized by the highest value of specific surface area and by intense exothermic phenomena at low temperature, as evidenced by the analysis of the solid residue. As a main conclusion, the processes involving nylon fibres that may modify the key parameters influencing the flammable/explosive behaviour are also discussed.

1. Introduction

Most studies dealing with dusts explosibility and flammability were performed assuming particle sphericity. However, combustible "non-traditional" dusts do not match this model, showing non-spherical shapes. Therefore, the study of the explosible properties of non-traditional dust may be challenging and requires to set specific procedures (Amyotte et al., 2012). Yet, it is highly demanded because of the widespread use of non-traditional dusts in the textile sectors as well as agriculture and food processing. Nylon is one of the most used synthetic polymers due to its high mechanical strength, flexibility, good stability under heat or chemical treatments. Thus, not only has it replaced silk and cotton to make fibres for textiles, but is also largely used to produce films for vacuum food packaging for oven, microwave or sous-vide allowing food to be packed, shipped, sold and cooked in the same packaging (Sirane Group, 2021). Nylon is produced starting from diamine acid, a monomer extracted from crude oil, that is combined with adipic acid to create a polymer (nylon salt crystals). The product is then heated to melting and extruded through a metal spinneret. The produced fibres are loaded onto a bobbin and stretched to increase their strength and elasticity. Finally, they are dyed and cut to produce the desired end product (Sewport, 2021). Both fibres and films fabrication involve production of short nylon fibres. For instance, the nylon films manufacturing process starts with melting down small nylon fibres, until they become molten and flattenable (Tricor Flexible Packaging Inc., 2021). Due to the presence of small nylon fibres, obtained by cutting longer nylon fibres loaded onto spool, a dust explosion may occur. Fibre explosibility has been occasionally investigated over the years and, consequently, there is a very low level of awareness of the risk of explosions due to these non-traditional dusts. Several authors highlighted

* Corresponding author.
E-mail address: maria.portarapillo@unina.it (M. Portarapillo).

https://doi.org/10.1016/j.jlp.2022.104815
Received 8 March 2022; Received in revised form 25 May 2022; Accepted 5 June 2022
Available online 14 June 2022

that flocculent materials displayed the same behaviour as spherical particles, explosion likelihood and severity increasing with a decrease in fibre diameter (Amyotte et al., 2011, 2012; Hossain et al., 2013; Russo et al., 2013; Worsfold et al., 2012). Moreover, Amyotte et al. (2012) and Marmo et al. (2018) examined the potential hazard of these materials as well as the experimental challenges posed by their marked flocculent nature. Nevertheless, the same authors underlined the lack of information about these samples, mainly regarding 20 L explosion chamber experimentations, and the lack of data on the fundamental ignition behaviour of flocculent dusts (Amyotte et al., 2012; Marmo et al., 2018). In our previous paper, we showed that the explosion mechanism of dusts occurs through the following network of series/parallel steps (Fig. 1) (Di Benedetto et al., 2010). Therefore, the explosion/flammability behaviour depends on the controlling step. According to the model developed by Di Benedetto et al. (2010) (Di Benedetto et al., 2010), the calculation of dimensionless numbers allows the identification of the controlling step. To calculate them and then to fully understand the explosion/-flammable behaviour of dusts, the evaluation of the thermal behaviour and the chemical nature is required. This work aims at fully characterising the flammability behaviour of nylon short fibres, that differs both for diameter and length as well as finishing surficial treatment. To this purpose, the ignition susceptibility analysis has been carried out to assess the minimum ignition energy (MIE), the maximum pressure of explosion and the deflagration index. Furthermore, an extensive chemico-physical characterization including the thermal behaviour has been performed by means of several techniques (TGA/DSC, FTIR, XRD). All these analyses have been used for the evaluation of several dimensionless numbers used to get insight into the step controlling the flame propagation in homogeneous and heterogeneous phase and consequently into the key features of the samples influencing the flame propagation, flammability and explosibility.

2. Materials and methods

Five nylon 6.6 samples with different properties summarised in Table 1 were investigated. Dtex (or decitex) is a unit of measurement for the linear density of fibres. It is equivalent to the mass in grams per 10,000 m of a single filament and can be converted to a particle diameter (Iarossi et al., 2013). Usually, nylon 6.6 fibres are covered by a thin layer of surfactant for production reasons. Consequently, they are sticky and do not disperse easily in the air. To remove the sticky layer, fibres are coloured and activated through a wet process. Moreover, the activation process alters the fibre surface and makes the fibres easy to suspend (Marmo and Cavallero, 2008).

Table 1
Properties and labels of nylon 6.6 samples.

Sample	Linear density (Dtex)	Activation	Colour	Label
Nylon 6.6	1.9	Yes	Blue	1
Nylon 6.6	3.3	Yes	No	2
Nylon 6.6	6.7	No	Dark blue	3
Nylon 6.6	6.7	Yes	Brown	4
Nylon 6.6	0.9	No	Dark blue	5

To identify the flame propagation controlling step, several dimensionless numbers have to be evaluated. Particularly, to assess the role of particle heating, we calculated the Biot number (*Bi*), which is the ratio between the internal heat conduction time (t_c) with respect to the external heat transfer time (t_e) (Equation (1)). The evaluation of the comparison between heat transfer and devolatilization reaction was performed by calculating the Damköhler number (*Da*), which is the ratio between the external heat transfer time (t_e) and the devolatilization chemical time (t_{pyro}) (Equation (2)). The thermal Thiele number (*Th*) allow the comparison between the conduction heat transfer time (t_c) and the pyrolysis chemical time (t_{pyro}) (Equation (3)). Notably, in the case of nylon, as well as for all non-traditional dusts, the dimensionless numbers have to be all evaluated by using D_{eq} as a representation of the dust size (Russo et al., 2013). To compare the volatiles combustion time to the pyrolysis time, the *Pc* number has to be evaluated as the ratio of the volatile combustion time (t_{comb}) and the pyrolysis time (t_{pyro}) (Equation (4)).

$$Bi = \frac{t_c}{t_e} = \frac{D_{eq}\cdot(h_c\cdot\Delta T_i + \varepsilon_\lambda\cdot\sigma\cdot\Delta T_i^4)}{\lambda_{dust}\cdot\Delta T_i} \quad (1)$$

$$Da = \frac{t_e}{t_{pyro}} = \frac{r_p\cdot\Delta T_i\cdot Cp_{dust}\cdot D_{eq}}{h_c\cdot\Delta T_i + \varepsilon_\lambda\cdot\sigma\cdot\Delta T_i^4} \quad (2)$$

$$Th = \frac{t_c}{t_{pyro}} = \frac{r_p\cdot Cp_{dust}\cdot D_{eq}^2}{\lambda_{dust}} \quad (3)$$

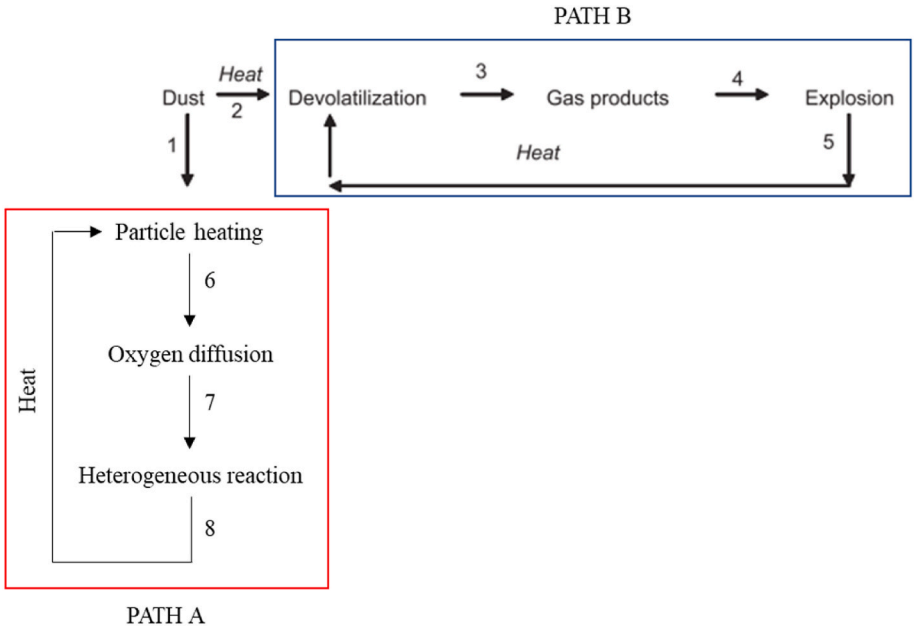

Fig. 1. *Schematic representation of the paths occurring during dust explosion* (Di Benedetto and Russo, 2007).

$$Pc = \frac{t_{pyro}}{t_{comb}} = \frac{\rho_{\mathrm{dust}} \cdot S_l}{r_p \cdot l_F} \tag{4}$$

where ΔT_i (K) is the temperature difference between particle and surrounding gases, h_c (W m^{-2} K^{-1}) is the heat transfer coefficient, ε_λ (−) is the emissivity, σ (W m^{-2} K^{-4}) is the Stefan–Boltzmann constant, λ_{dust} (W m^{-1} K^{-1}) is the thermal conductivity of the solid, r_p (kg/m^3 s) is the pyrolysis reaction rate, Cp_{dust} (J kg^{-1} K^{-1}) is the specific heat, l_F is the flame thickness (typically, 1 mm), ρ_{dust} (kg/m^3) is the dust density and S_l (m/s) is the laminar burning velocity. *Pc* number was calculated by assuming S_l = 0.2 m/s. Moreover, two additional dimensionless numbers have to be considered to assess the step controlling the heterogeneous combustion. More precisely, the Thiele modulus (Φ_{Th}) indicates the rate of reaction with respect to the rate of intra-particle diffusion while the Sherwood number (*Sh*) represents the ratio of the inter-particle (convective) mass transfer to the rate of intra-particle mass diffusion transport. The Thiele modulus (φ_{Th}) for a first order reaction can be calculated as follows:

$$\varphi_{Th} = D_{eq}\sqrt{\frac{k_{in}}{D_{O_2}}} \tag{5}$$

The Sherwood number is a function of the Reynolds and Schmidt dimensionless numbers (Ranz and Marshall Jr., 1952; Rowe et al., 1965):

$$Sh = Kc \cdot \frac{D_{eq}}{D_{O_2}} = 2 + 0.69 Re^{\frac{1}{2}} Sc^{\frac{1}{3}} \tag{6}$$

where k_{in} (s^{-1}) is the intrinsic kinetic constant for the first exothermic peak found in oxidative atmosphere, D_{O2} (m^2/s) is the effective oxygen diffusivity, *Kc* (m/s) is the external mass transfer coefficient and *Sc* (−) is the Schmidt number defined as

$$Sc = \frac{\mu}{\rho D_{O_2}} \tag{7}$$

SEM analysis was carried out through Philips mod. XL30 at magnifications from 100× to 6000×. From these images, the shape of the dust was identified. In addition, ImageJ was used to estimate particle sizes by means of a statistical analysis. To determine both the crystallographic structure and the degree of crystallinity, XRD analysis was carried out through XRD diffractometer PANalytical X'Pert Pro using Cu Kα radiation (1.5406 Å). The range of variability of 2θ is [5°; 79.99°] with a step size of 0.013° and a scan step time of 8.67 s. The calculation of interplanar spacing (d) was calculated through Bragg's law (Bragg and Bragg, 1913) while the average crystal size (D) was determined by Debye-Scherrer equation (Debye and Scherrer, 1916). BET theory aims to explain the physical adsorption of gas molecules on a solid surface and serves as the basis for an important analysis technique for the measurement of the specific surface area (SSA) of materials. During this analysis, the density of the material can also be evaluated. BET SSAs were measured by N_2 adsorption at 77 K with a Quantachrome Autosorb-1C instrument after degassing the samples at 150 °C for 1.5 h. The device MIKE3 was used to estimate minimum ignition energy of dust samples (ASTM International, 2003). It consists of a 1.2 L volume vertical glass tube. The bottom is made of stainless steel and it is shaped to act as a dust distributor. A mushroom-shaped air nozzle, provided with seven holes for air flow, is in the middle of the distributor. Two tungsten electrodes are located at 1/3 height from the bottom of the test chamber. The tips of the electrodes are located symmetrically with respect to the vertical axis of the test chamber. The two tips are 6 mm apart. The top of the test chamber is closed with a disk of filter paper held in place in such a way that the explosion can open the test chamber to vent the explosion products. The device can control the delivered energy and the delay time between the dust suspension and the spark. The delay time can be varied between 30 and 180 ms. In this work, the standard delay time has been used (120 ms) with an inductance at 1 mH. Each sample was submitted to a maximum of ten ignition attempts at different concentrations and delivered energy.

The standard 20 L explosion vessel was used to determine $P_{\max}$, $(dP/dt)_{max}$ and K_{St} (ASTM E1226-19, 2019). Due to the low bulk density of the samples, for all the tested concentrations, the sample was placed directly in the 20 L vessel around the rebound nozzle used for dust dispersion, as suggested in Amyotte et al. (2012). In particular, Amyotte et al. (2012) developed a test procedure for the 20-L chamber in which a maximum of 15 g of dust were placed in the external dust storage container and the remaining part was charged directly around the rebound nozzle. In this work, we observed an obstruction of the external electro-pneumatic valve already at 250 g/m^3 (5 g sample). For this reason, we decided to charge the whole amount of sample around the rebound nozzle. It is worth noting that in this case all the measurements were repeated three times but all the results must be taken into account as qualitative and not quantitative since the tests were not carried out following the recommendation of the standard description (ASTM E1226-19, 2019). Moreover, for all the samples, it was necessary to perform a manual evaluation to identify the maximum rate of pressure rise due to the flock explosion, always weaker than the chemical igniters explosion. Indeed, as shown in Figure S1, the chemical igniters explosion is always more severe than the flock explosion and the software evaluation of the maximum rate of pressure rise is always relative to chemical igniters explosion phenomenon.

To evaluate thermal properties and characteristic temperatures of the samples and assess some parameters useful for the dimensionless number evaluation, thermogravimetric analyses were carried out with TGA/DSC TA instrument Q600SDT. 5 mg sample were loaded into an alumina pan and were tested up to 1000 °C (heating rate 10 °C/min) in both inert (N_2) and oxidative (air) atmosphere (flow rate 100 mL/min). Through TG/DSC analyses in inert atmosphere, some key information about the homogeneous path may be derived such as the volatile content, the heat of devolatilization and the released gaseous species composition. Conversely, with tests in oxidative atmosphere, the heterogeneous path may be investigated, the chemical interaction of the dust with oxygen.

From TG analysis, the proximate analysis determined the moisture content (M), volatile matter (V), ash (A) and the calculation of fixed carbon (H), following the standard procedure (ASTM D7582 - 15, 2015). Gases produced from samples degradation, were analysed through FTIR gas spectroscopy which was carried out through TGA/FTIR interface in line coupled with to TGA furnace. The cell and transfer line of the TGA/FTIR interface were heated and kept at 220 °C. In this way, product gases from samples degradation could not condense. The output of this analysis is a Gram-Schmidt diagram. The HR Nicolet TGA Vapor Phase library of OMNIC software has been used to recognize the product gases. To confirm the chemical nature of the substances and to exclude differences due to colouring and activation processes, FTIR analysis was carried out on solid samples through Nicolet 5700 FTIR, solid (KBr grade), disk 1%, resolution 4 cm^{-1}, range 4000–400 cm^{-1} out with.

3. Results

3.1. SEM analysis

SEM analysis was carried out to assess the fibre shape, length and diameter. Fig. 2 shows SEM images for all investigated dusts at different magnifications. All the samples are composed by cylindrical fibres. From these images, it is not possible to notice the differences due to the dying, whereas the effects of the activation process are evident. In particular, fibres of samples 1, 2 and 4 appear well separated because the surfactant thin layer has been removed by the wet activation process. Conversely, fibers in samples 3 and 5, both not activated, are more compact. Especially in 200× SEM image of sample 3 (Fig. 2 (c)), a sticky group of fibers is easily visible. Average length and diameter of fibres were calculated from the SEM images, by statistical analysis using ImageJ program

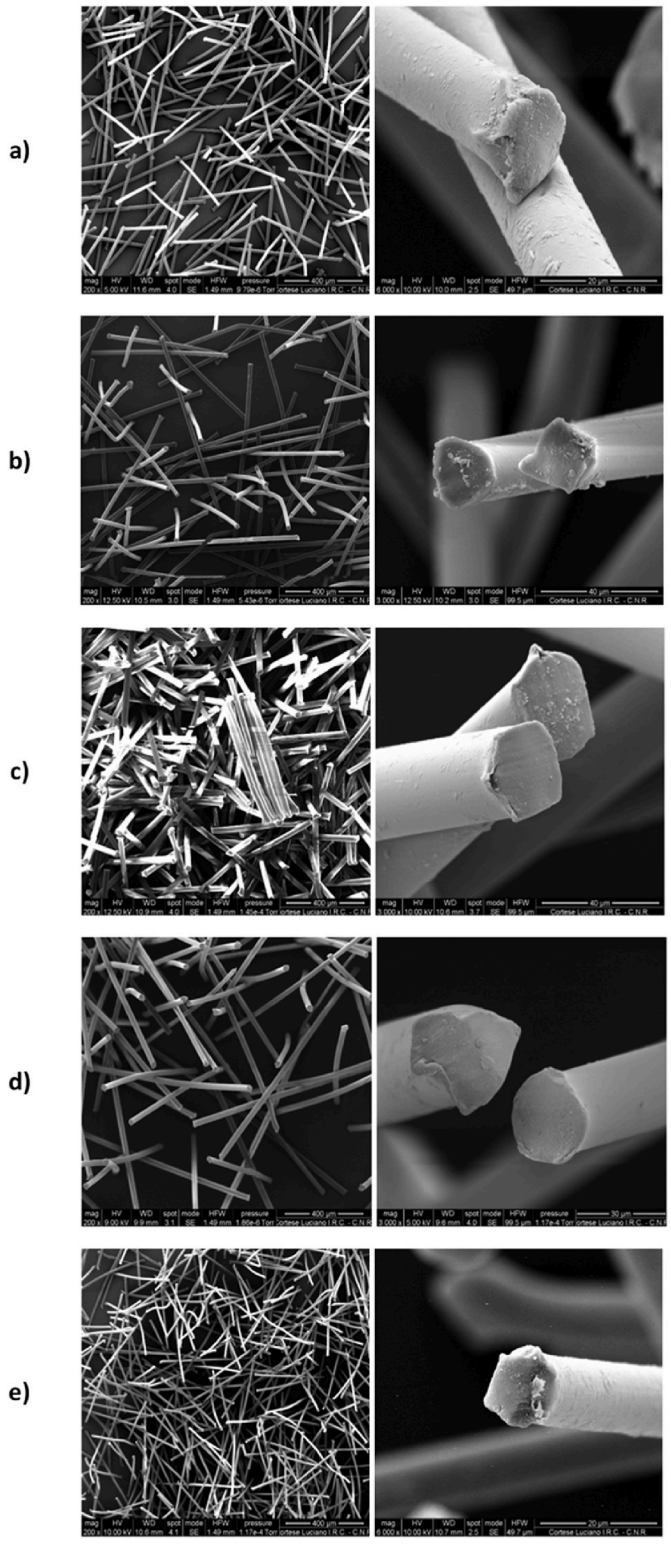

Fig. 2. SEM images of sample 1 (a), sample 2 (b), sample 3 (c), sample 4 (d) and sample 5 (e) investigated at 200× (left) and 6000× (right) magnification.

(Schneider et al., 2012) (Table 2).

The fibre diameter and length ranges from 10 up to 30 μm and 319 up to 933 μm, respectively. Furthermore, sample 1 and 5 show the smallest diameter and length. Table 2 also reports the equivalent particle diameters, D_{eq} as calculated according to the following formula (Russo et al., 2013):

Table 2
Average length and diameter of nylon 6.6 fibres.

Sample	Linear density (Dtex)	Length, L (μm)	Diameter, d_f (μm)	D_{eq} (μm)
1	1.9	393	15	87
2	3.3	520	20	115
3	6.7	540	30	144
4	6.7	933	30	189
5	0.9	319	10	64

$$D_{eq} = 2\sqrt{\frac{d_f L}{\pi}} \tag{8}$$

The smallest value of the equivalent diameter is found for sample 5.

3.2. Flammability

The flammability of nylon 6.6 fibres was investigated, by measuring the minimum ignition energy in the Hartmann tube at 120 ms and 1 mH. In Table 3, MIE or E_s values are reported, as measured for all the nylon 6.6 samples. Samples 2, 3 and 4 did not ignite for ignition energy equal up to 1000 mJ. Sample 5 is the most susceptible to electric discharge ignition followed by sample 1. As found with SEM analysis, these samples are characterized by the smallest values of equivalent diameters.

3.3. Explosibility

Table 4 shows the values of maximum pressure of explosion, maximum rate of the pressure rise and deflagration index, which were obtained testing the samples with the standard procedure (ASTM E1226-19, 2019), modified for the case of fibres. As it can be observed, Sample 5 is not only the most sensitive to ignition but also the most explosive, although all the samples turn out to be class St-1 explosives.

3.4. FTIR analysis

All the samples have been characterized by FTIR analysis to identify their chemical nature. Figure S2 shows the FTIR spectra are shown as obtained for all samples. The spectrum of Nylon 6,6 is also shown for comparison. The bands of the spectra are given in Table S1. The spectra of all samples (1–5) correspond to the spectrum of nylon 6.6 (Hummel Polymer Sample Library of OMNIC software).

3.5. BET analysis

Table 5 reports the specific surface area (SSA) measured through BET analysis as well as sample density. SSA values are quite similar except for sample 3 and 5 which exhibit the lowest and the highest specific surface area, respectively. The densities of each sample are comparable except for sample 1 one which shows a slightly higher value. From these first analyses, as expected, the explosive behaviour seems to strongly depend on the sizes of the fibres. Small sizes make fibre dispersion easier and more effective. This phenomenon makes the formation of an explosive cloud more probable. Notably, the surface area also play a role in determining the explosive behaviour. The specific surface area (SSA) is a key parameter which significantly affects the heat transfer rate, the volatilization rate, the heterogeneous combustion and most importantly

Table 3
Minimum Ignition Energy of nylon 6.6 samples, tv = 120 ms and L = 1 mH.

Sample	E_1 (mJ)	E_s (mJ)	E_2 (mJ)
1	300	471	1000
2	–	–	>1000
3	–	–	>1000
4	–	–	>1000
5	100	228	300

Table 4
P_{max}, $(dP/dt)_{max}$ and K_{St} of nylon 6.6 samples, IE = 10 kJ.

Sample	P_{max} (bar)	$(dP/dt)_{max}$ (bar/s)	K_{St} (bar m/s)
1	6.6	180	50
2	6.4	110	30
3	6.6	80	22
4	5.2	40	11
5	7.0	250	68

Table 5
Specific surface area and density of nylon 6.6 samples.

Sample	SSA (m^2/g)	Density (g/cm^3)
1	10.5	1.23
2	10.4	1.07
3	3.9	1.11
4	10.8	1.05
5	14.3	1.06

O_2 diffusion. Oxygen diffusion is also affected by crystalline fraction of materials. Indeed, a low crystalline degree (amorphous material) promotes the diffusion of oxygen that can sustain the combustion reaction thus supporting the flame propagation (Nabatame et al., 2003). The calculation of crystalline fraction for all the samples will be showed and discussed in the following sections. Instead, activation ad coloration seems to have slight effect on the explosive character, negligible compared to the effect of the size of the fibers. Indeed, sample 5 is the most reactive even if its dispersibility is compromised due to the absence of the activation process. It can be concluded that in the case of sample 5, the dispersion is effective despite the absence of the activation process due to the small size which plays a fundamental role. Therefore, activation ad coloration will considered as negligible in the rest of the study. To correlate the chemical/physical properties to the flammability feature, it is interesting to evaluate the thermal behaviour of nylon 6.6 samples in N_2 and oxidative atmosphere.

4. Thermal analysis

4.1. Proximate analysis

Proximate analysis was performed on each sample to quantify the volatile (V), the humidity (M), the ash (A) and the fixed carbon (F) contents (ASTM D7582 - 15, 2015). Obtained values are reported in Table 6, for all samples. The moisture percentage is about 1% for all samples. The volatile content is very high ranging from 90 to 98%. The ash content is lower than 10% for all samples, while fixed carbon is not present. From these data we may conclude that all the samples have a very high volatile content. In our previous papers, we showed that the dust response to the temperature increase is very useful for understanding the phenomena controlling the flammability/explosion behaviour of dusts (Centrella et al., 2020; Portarapillo et al., 2020). In this work, we performed thermogravimetric analysis of all samples, in both N_2 and air atmosphere. The temperature has been varied up to 600 °C, at a heating rate equal to 10 °C/min.

Table 6
Proximate analysis of nylon 6.6 samples (ASTM D7582 - 15, 2015).

Sample	M%	V%	A%	F%
1	0.3	98.7	1.0	≈0
2	1.1	96.5	2.4	≈0
3	1.1	98.7	0.2	≈0
4	0.4	91.0	8.6	≈0
5	0.7	92.3	7.0	≈0

4.2. N_2 atmosphere

TG curves for all samples are reported in Figure S3, in terms of weight loss as function of temperature are shown as obtained for all the samples. From these profiles, characteristic temperatures were calculated: the onset temperature at which weight loss starts (T_{onset}), the inflection point temperature at which there is the maximum rate of weight decrease (T_{flex}) and the temperature at which the weight loss ends (T_{offset}). The calculated values are reported in Table 7. Sample 5 has an early thermal degradation (380 °C) compared to the others (≈390 °C). This could be due to the lowest fibre sizes. The maximum degradation rate is also reached earlier (T_{flex}), about 10 °C, by sample 5. In addition to the TG curves, DSC curves in nitrogen atmosphere are reported in Fig. 3.

Two endothermic peaks are found for all samples. The former peaks (256 °C) can be addressed to the melting of the crystalline material. The temperature of the second (endothermic) peak is slightly different for all samples and it is equal to the flex temperature (T_{flex}). This peak has been addressed to the occurrence of a pyrolysis reaction. To evaluate the nature of the produced gas, FTIR gas analysis was carried out and the obtained the Gram-Schmidt diagram is shown in Figure S4. All samples exhibit a single peak which corresponds to the temperature of the second peak in the DSC diagrams (Fig. 3), confirming the occurrence of the pyrolysis reaction. At each peak of Gram-Schmidt diagram corresponds a spectrum shown in Fig. 4.

All curves have the same main peaks. Noteworthy, decomposition of all samples leads to the formation of the same volatile substances. In particular, CO_2 (peaks between 2400 and 2200 cm^{-1} and at 669 cm^{-1}), NH_3 (peaks at 3330 cm^{-1} and between 2000 and 600 cm^{-1}) and H_2O (peaks in bands 4000-3000 cm^{-1} and 2200-500 cm^{-1}) are the main products in N_2 atmosphere measurements. Moreover, the two peaks at 2934 and 2866 cm^{-1} are due to C–H bond, so they indicate a hydrocarbon chain while the peak at 1766 cm^{-1} is related to C═O bond, related to the production of cyclopentanone (Hornsby et al., 1996).

4.3. Air atmosphere

The tests in air have been carried out up to 600 °C with heating rate equal to of 10 °C/min. TG curves for all samples are shown in Fig. 5.

The TG curves in oxidative atmosphere are significantly different from those obtained in N_2. Several additional weight losses are observed. Table 8 shows different onset, offset and inflection temperatures as many as the phenomena occurring for each sample.

Focusing on sample 5, it is characterized by the lowest value of onset temperature, thus, its thermal decomposition as well as interaction with oxygen start at lower temperature. The first weight loss of sample 5 is the highest, with a weight loss of 40% at temperature below 342 °C ($T_{offset,1}$). It is worth noting that between $T_{offset,1}$ and $T_{onset,2}$ of sample 5 there are about 100 °C in which the sample actually continues to lose weight (about 20%) with a slower phenomenon than the first and third ones, with the latter which ends with the complete consumption of the solid within 500 °C. Fig. 6 shows the corresponding DSC curves as

Table 7
Characteristic temperatures from TG curves in N_2 atmosphere.

Sample	T_{onset} (°C)	T_{flex} (°C)	T_{offset} (°C)
1	390	427	510
2	391	429	495
3	387	425	507
4	392	430	493
5	380	417	510

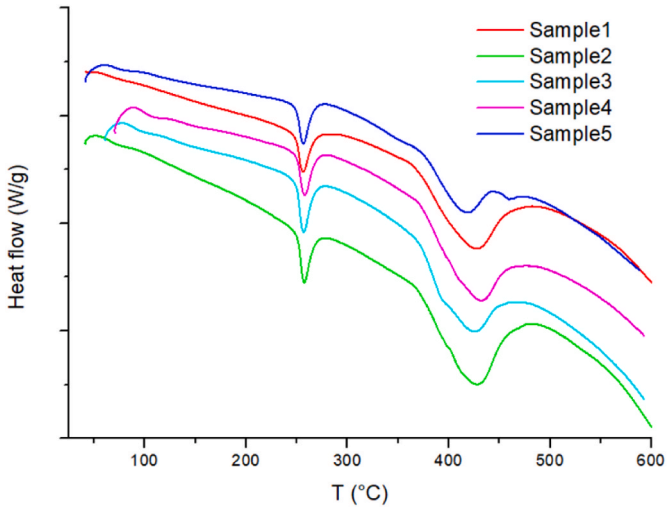

Fig. 3. DSC curves of nylon 6.6 samples in N_2 atmosphere.

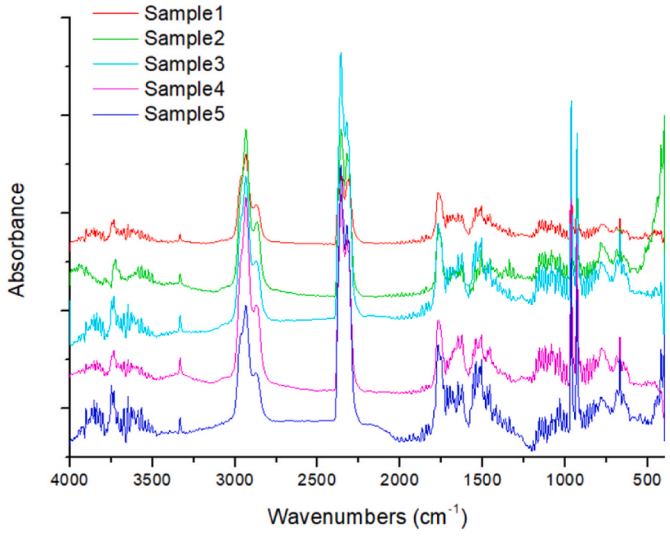

Fig. 4. Spectra of product gases during pyrolysis of nylon 6.6 samples.

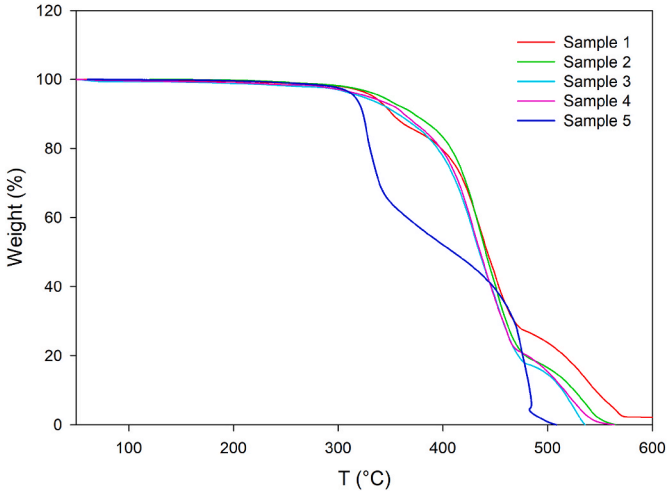

Fig. 5. TG curves of nylon 6.6 samples in oxidative atmosphere (air), 10 °C/min.

obtained for each sample.

All samples exhibit a first endothermic peak which can be addressed to the crystalline melting of the material (as in the N_2 measurement). Furthermore, several exothermic peaks are evident unlike DSC curves recorded in N_2 atmosphere. In the case of sample 5 these peaks are the highest among investigated samples. Table 9 shows the peak temperature ($T_{Iexopeak}$) and the released heat ($\Delta H_{Iexopeak}$) in correspondence of the first exothermic peak, for all samples.

It is worth noting that the heat released at the first peak, increases as the characteristic fibre dimension (D_{eq}) decreases. To assess the chemical nature of the solid residue after the first exothermic peak, FTIR analysis was performed. For samples 1, 2, 3, 4, the residue had a very tough shell. However, inside the shell, the substance present is still nylon 6.6 as reported in the spectra of Figure S5. The residue of sample 5 had a porous and easy to pulverize shell. As can be seen in Fig. 7, the spectrum of sample 5 after the first exothermic peak, (Sample5_afterIexopeak) is significantly different from that of nylon 6.6 and very similar to the spectrum of char (Xia et al., 2015), suggesting that a chemical transformation has occurred.

As can be seen in Fig. 6, at 400 °C, other exothermic reactions occur in the case of the other samples. DSC and FTIR results suggests that after the first peak, a surface hard is formed which isolates the nylon core until, at high temperatures, the shell breaks allowing the diffusion of oxygen and then the heterogeneous reaction. To evaluate the chemical nature of the gaseous substances released during the first peak, FTIR on evolved gas was carried out. Figure S6 shows the Gram-Schmidt profiles as functions of time and temperature for each sample. All Gram-Schmidt diagrams show two main peaks, the former recorded during the exothermic phenomenon in DSC analysis. The spectra of evolved gases are reported in Fig. 8.

From the comparison between FTIR spectra, it can be driven that there are some differences between the composition of evolved gases in oxidative (Fig. s9; S7-S9) and inert atmosphere (Fig. 5). In particular, Figure S7 shows FTIR spectra of the volatile substances produced by sample 1 evidencing that CO_2 (at 2400-2200 cm^{-1}) and H_2O (at 4000-3400 cm^{-1} and 2000-1200 cm^{-1}) are the main products, with CO in trace (at 2200-2000 cm^{-1}). Thus, differently from the results under N_2 atmosphere, cyclopentanone was not found. Figure S8 shows the FTIR spectra of samples 2, 3 and 4, which evidence that. The main product is CO_2. The peaks at 2960 cm^{-1} and at 2252 cm^{-1} can be addressed to metyl-isocyanate (C_2H_3NO), whereas the bands at 2181 and 2106 cm^{-1} suggest the presence of CO. Furthermore, the peaks at about 1750 cm^{-1} suggest the presence of small amount of cyclopentanone. Moreover, in the case of Sample 5 the formation of CO (green) and NH_3 (red) is detected (Figure S9). The peak at 1766 cm^{-1} is related to C═O bond (production of a significant amount of cyclopentanone) while bands at 2181 and 2106 cm^{-1} are due to CO. As for samples 2, 3 and 4, the peaks at 2960 cm^{-1} and at 2252 cm^{-1} are attributable to metyl-isocyanate (C_2H_3NO). The interaction with oxygen of Sample 5 at low temperature (the onset temperature in oxidative atmosphere is about 300 °C) leads to the generation of combustible volatiles (CO, NH_3, C_2H_3NO and cyclopentanone). It is worth noting that although in the oxidizing environment the main products are those typical of complete combustion (CO_2 and water) due to the presence of the combustion reaction in the heterogeneous phase, even in oxidative atmosphere there is still the formation of flammable gaseous species produced by thermal decomposition of the fibres that can take part to combustion in the homogeneous phase. In order to better clarify the reason why sample 5 is the most reactive, we evaluated the step controlling the sample ignition/explosion.

4.4. Evaluation of the controlling step

To assess all the dimensionless numbers, the pyrolysis kinetics and the thermal trends in oxidative atmosphere were studied in detail. The Flynn−Wall−Ozawa (FWO) method was used to calculate the activation

Table 8
Characteristic temperatures from TG curves in oxidative atmosphere (air), 10 °C/min.

Sample	$T_{onset,1}$ (°C)	$T_{flex,1}$ (°C)	$T_{offset,1}$ (°C)	$T_{onset,2}$ (°C)	$T_{flex,2}$ (°C)	$T_{offset,2}$ (°C)	$T_{onset,3}$ (°C)	$T_{flex,3}$ (°C)	$T_{offset,3}$ (°C)
1	325	344	357	414	436	472	512	538	571
2	396	434	469	514	533	567	–	–	–
3	391	432	471	506	523	548	–	–	–
4	390	431	465	500	518	562	–	–	–
5	318	328	342	450	474	483	483	493	500

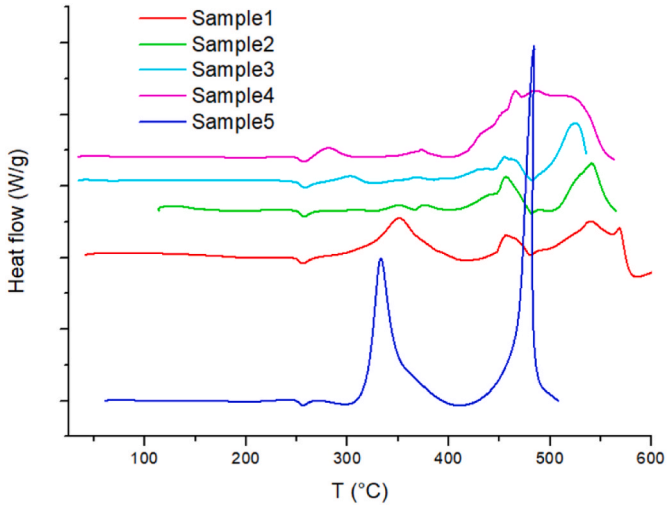

Fig. 6. DSC curves of nylon 6.6 samples in oxidative atmosphere.

Table 9
Temperatures and heat released at first exothermic peak of each sample. The equivalent diameter is also reported.

Sample	D_{eq} (μm)	$T_{1exopeak}$ (°C)	$\Delta H_{1exopeak}$ (J/g)
1	87	351	−233.0
2	115	350	−12.6
3	144	305	−14.4
4	189	282	−27.4
5	64	334	−508.6

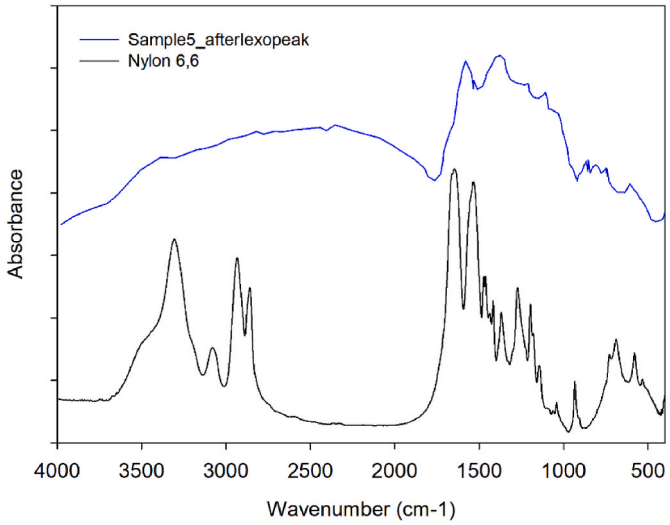

Fig. 7. Spectra of nylon 6.6 TQ (black) and sample 5 (blue) after the first exothermic peak.

energy E_a and Arrhenius pre-exponential factor Z values (Liu et al., 2020). The kinetic analysis is fully reported in the Supplementary Material file (Figure S10-S17). Table 10 reports the kinetic parameters of pyrolysis reaction which consists of a single stage for each sample. As shown in Table 10, the activation energy (E_a) and the intrinsic kinetic constant (Z) are the same for all samples, except for sample 5, suggesting that a different mechanism is occurring when the sample undergoes pyrolysis.

In Table 11, the external heat transfer coefficient, the fibre equivalent diameter and the effective oxygen diffusivity are reported for each sample. Table 12 contains the values of *Bi*, *Da*, *Th* and Pc as calculated for all samples, where $h_c = \frac{\lambda}{D_{eq}}$ is the heat transfer coefficient with the model of pipe wall.

The other parameters to calculate dimensionless numbers are (Professional Plastics, n.d.):

- $Cp_{dust} = 1670$ J/kg K
- $\lambda_{dust} = 0.25$ W/m K
- $\varepsilon_\lambda = 0.88$
- $\Delta T = 0.5$ K value chosen due to the fibres size
- $\sigma = 5.67 \times 10^{-8}$ W/m^2 K^4

Biot number is equal to 1 for all the samples, suggesting that external and conduction (internal) heat transfer time are comparable. *Da* and *Th* numbers are found to be both much lower than 1, for all samples. From the values of *Pc* (≫1) we may conclude that the pyrolysis time is much higher than the volatile combustion time then identifying the pyrolysis of nylon 6,6 as the controlling step of the flame propagation. However, the pyrolysis time strongly depends on the fibre size.

Table 12 shows the pyrolysis time ($t_{pyr} = \rho_{dust}/rp$) for each sample, with a value quite lower in the case of Sample5, which proved to be the most sensitive to ignition (lowest value of the MIE). As a result, when the pyrolysis is faster, the dust is more flammable and the explosion that occurs is more severe.

As far as it regards the analysis in oxidative atmosphere, the kinetic analysis was more complex due to the presence of several phenomena occurring at different temperatures and heating rates (e.g., oxygen diffusion, heterogeneous combustion, devolatilization etc.). For all the samples except Samples 3 and 4, it was possible to focus on three different stages and the respective kinetic parameters were evaluated. The kinetic analysis is fully reported in the Supplementary Material file (Figure S18-S32).

For the calculation the Thiele modulus (φ_{Th}), the intrinsic kinetic constant (k_{in}) was evaluated by considering the effectiveness factor η and the Weisz–Prater module Φ, so that the effect of oxygen mass transfer can be evaluated and eliminated (Zhao and Sun, 2013). *Sh* was calculated assuming Reynolds number equal to 2000 (i.e., the maximum value allowable by Equation (6) by (Ranz and Marshall Jr., 1952; Rowe et al., 1965).

The effective oxygen diffusivity was calculated for each sample using Equation 9

$$D_{O_2,i} = \left(\frac{100 - X_c}{100}\right)^2 D_a \, T_{peak}^{3/2} \tag{9}$$

where X_c is the crystalline fraction within the sample and D_a (m^2/s) is the oxygen diffusion coefficient of the amorphous polyethylene ($Xc = 0$)

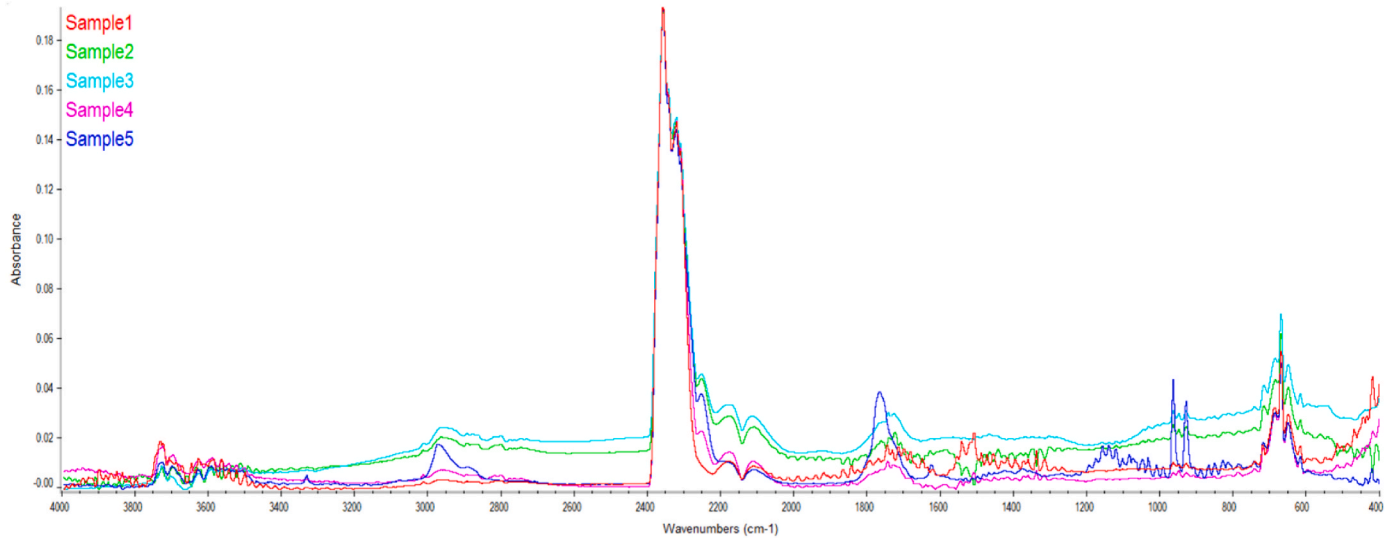

Fig. 8. Spectra of product gases at first exothermic peak of nylon 6.6 samples.

Table 10
– Kinetic parameters relative to decomposition in inert atmosphere for each sample.

Sample	D_{eq} (μm)	T_{peak} (K) 5 °C/min	T_{peak} (K) 10 °C/min	T_{peak} (K) 20 °C/min	E_a (kJ/mol)	Z (s^{-1})
1	87	675	698	718	≈169.0	3.2×10^{10}
2	115	675	698	718	≈169.0	3.2×10^{10}
3	144	675	698	718	≈169.0	3.2×10^{10}
4	189	675	698	718	≈169.0	3.2×10^{10}
5	64	671	689	708	≈176.5	1.8×10^{11}

Table 11
Hydraulic diameter and heat transfer coefficient of nylon 6.6 samples.

Sample	L (μm)	d_f (μm)	D_{eq} (μm)	h_c (W/m^2 K)
1	393	15	87	2499.0
2	520	20	115	2172.5
3	540	30	144	1740.7
4	933	30	189	1324.3
5	319	10	64	3922.7

Table 12
Dimensionless numbers for all samples and pyrolysis time.

Sample	Bi	Da	Th	Pc	t_{pyr} (s)
1	1	4.42×10^{-4}	4.42×10^{-4}	2.84×10^{4}	1.41×10^{2}
2	1	7.72×10^{-4}	6.72×10^{-4}	2.82×10^{4}	1.41×10^{2}
3	1	1.21×10^{-3}	1.09×10^{-3}	2.82×10^{4}	1.41×10^{2}
4	1	2.09×10^{-3}	1.78×10^{-3}	2.82×10^{4}	1.41×10^{2}
5	1	2.39×10^{-4}	2.14×10^{-4}	2.71×10^{4}	1.36×10^{2}

at ambient temperature (1.70×10^{-10} m^2/s) (Michaels and Bixler, 1961). To estimate X_c, we calculated the fusion heat ΔH^{fus}_{sample} from the DSC analysis for each sample:

$$X_c = \frac{\Delta H^{fus}_{sample}}{\Delta H^{fus}_{nylon}} \quad (10)$$

where ΔH^{fus}_{nylon} (J/g) is the heat of fusion of crystalline nylon 6,6 (175.6 J/g) (Starkweather et al., 1984). In Table 13, the heats of fusion and the crystalline fractions are reported.

Table 13
Heats of fusion and the crystalline fractions of nylon 6.6 samples.

Sample	D_{eq} (μm)	ΔH^{fus}_{sample} (J/g)	X_c (−)
1	87	63.94	0.36
2	115	68.57	0.39
3	144	69.28	0.39
4	189	70.76	0.40
5	64	53.27	0.30

The evaluation of the crystallinity degree is very important since it has been shown that amorphous materials have oxygen diffusion coefficient much higher than crystalline materials (Nabatame et al., 2003), thus increasing the reaction rate of the heterogeneous path which is mainly controlled by O_2 diffusion. Therefore, the reactivity of dusts should increase with the lower crystalline degrees. Sample 5 is characterized by the lowest crystalline fraction thus, at the same temperature, it is characterized by the highest value of oxygen diffusivity.

XRD analysis was carried out to assess crystal sizes and patterns are shown in Figure S33. According to Diaz-Alejo et al. (2013) (Diaz-Alejo et al., 2013), the samples show a similar diffraction pattern of a predominant amorphous material with some crystallinity degree as conferment by the presence of melting peak in DSC curve. The peaks at around $2\theta = 19°$ and $2\theta = 26°$ correspond to the reflection of (100) and (010,110) doublet of the α phase of nylon 6.6 crystals oriented in a triclinic cell. From this analysis, average crystal size (D) and interplanar spacing (d) were calculated by Debye-Scherrer equation (Debye and Scherrer, 1916) and Bragg law (Bragg and Bragg, 1913), respectively. These parameters are reported in Table S2. The interplanar spacing lies between 3.5 and 4.5 Å while the average crystal size changes a lot from sample to sample. Sample 5 shows the lowest pair of parameters.

In Table 14, the kinetic parameters of oxidation reactions are reported while all the dimensionless numbers have been calculated and showed in Table 15. From the obtained values of Φ_{Th} ($\ll$1), we may conclude that the heterogeneous flame propagation path is controlled by the intrinsic reaction. Consequently, the main effect is played by the specific surface area. Sample 5, that has the highest value of *SSA*, reacts faster and at lower temperature compared to the other samples.

5. Discussion

To summarize, it is possible to have the nylon fibres intrinsically safe by controlling three key factors:

Table 14
Kinetic parameters, oxidative atmosphere.

Sample	D_{eq} (μm)	First stage					Second stage					Third stage				
		T_{peak} (K) 2 °C/min	T_{peak} (K) 5 °C/min	T_{peak} (K) 10 °C/min	T_{peak} (K) 20 °C/min	E_a (kJ/mol)	T_{peak} (K) 2 °C/min	T_{peak} (K) 5 °C/min	T_{peak} (K) 10 °C/min	T_{peak} (K) 20 °C/min	E_a (kJ/mol)	T_{peak} (K) 2 °C/min	T_{peak} (K) 5 °C/min	T_{peak} (K) 10 °C/min	T_{peak} (K) 20 °C/min	E_a (kJ/mol)
1	87	583	606	–	–	95.3	733	763	–	–	80.7	800	833	–	–	148.4
2	115	582	604	–	–	106.3	734	774	–	–	86.8	809	853	–	–	160.9
3	144	–	689	703	718	210.3	–	–	–	–	–	–	–	–	–	–
4	189	–	690	705	719	206.5	–	–	–	–	–	–	–	–	–	–
5	64	–	593	603	619	147.8	–	649	673	693	94.7	–	740	751	773	167.9

Sample	Z (s^{-1})	Z (s^{-1})	Z (s^{-1})
1	3.94×10^{5}	3.40×10^{2}	4.62×10^{6}
2	4.43×10^{6}	9.74×10^{2}	2.47×10^{7}
3	3.5×10^{13}	–	–
4	1.71×10^{13}	–	–
5	5.23×10^{10}	9.40×10^{4}	6.10×10^{6}

Table 15
Dimensionless numbers for all sample, oxidative atmosphere.

Stage	Sample	D_{O2} (m^2/s)	Φ_{Th}	Sh
I	1	9.68×10^{-7}	3.42×10^{-3}	$7.88\times10^{+1}$
	2	8.87×10^{-7}	4.34×10^{-3}	$8.10\times10^{+1}$
	3	1.16×10^{-6}	1.20×10^{-2}	$7.43\times10^{+1}$
	4	1.13×10^{-6}	1.63×10^{-2}	$7.49\times10^{+1}$
	5	1.22×10^{-6}	5.19×10^{-3}	$7.31\times10^{+1}$
II	1	1.36×10^{-6}	2.10×10^{-3}	$7.06\times10^{+1}$
	2	1.26×10^{-6}	2.60×10^{-3}	$7.25\times10^{+1}$
	3	–	–	–
	4	–	–	–
	5	1.44×10^{-6}	3.43×10^{-3}	$6.93\times10^{+1}$
III	1	1.56×10^{-6}	2.45×10^{-3}	$6.77\times10^{+1}$
	2	1.45×10^{-6}	3.01×10^{-3}	$6.92\times10^{+1}$
	3	–	–	–
	4	–	–	–
	5	1.70×10^{-6}	1.74×10^{-4}	$6.58\times10^{+1}$

1. size of the fibres that regulates the dispersibility and the pyrolysis time;
2. specific surface area which controls the heterogeneous reaction rate;

5.1. Degree of crystallinity that influences the oxygen diffusivity

Large dimensions of the fibres characterized by limited surface areas (therefore low porosity) and relevant amorphous fraction should be guaranteed in every step of the nylon production process.

Unfortunately, during the production of nylon fibres the formation of small nylon fibres is inevitable (Sewport, 2021).

The explosion risk would be significantly reduced if the dimensions of the fibres are limited to D > 30 μm and L > 0.5 mm. It is worth noting that in this work we studied the effect of dimensions by looking at the equivalent diameter parameter. In a previous work, Marmo and Cavallero (2008) found that the influence on MIE of the diameter is more marked with respect to the length (Marmo and Cavallero, 2008). However, the fibers length greatly influences the dispersibility of the fibers within a confined environment and, moreover, it is the parameter that can be most easily modified and reduced during the processing of nylon fibers. For this reason, we have decided to take into account the effect of fibres size in terms of equivalent diameter always considering that generally the diameter plays a more significant role on the flammability and explosiveness of non-traditional powders than the fibers length.

Frequently, to increase the interfacial adhesion performance of nylon-rubber composites with high mechanical resistance, the nylon fibres are subjected to surface treatments with chemical agents (e.g., formic acid) eventually increasing the surface roughness (Krishna Prasad et al., 2017; Krump et al., 2005; Maher and Wardman, 2015; Zille et al., 2015). These treatments increase the porosity (formation of roughness containing pits, cracks and micropores) as a function of the concentration of the chemical agent. Consequently, the surface area of the treated samples would result higher than the untreated sample and would cause a faster heterogeneous reaction in case of ignition. Since the flame propagation in the heterogeneous phase for these materials is controlled by the intrinsic reaction, the effects of any surface treatments must be *a priori* evaluated. Notably, the superficial treatments most likely modify the surface to the order of submicron level without affecting the bulk properties.

Other surface treatments such as ablation and etching involve significant attack both in the para-crystalline regions or in the crystalline regions (Okuno et al., 1992). Specifically, these treatments may reduce the characteristic size of the fibres and also change the amorphous fraction of the material, influencing the oxygen diffusion through the

combustible fibres (Kim et al., 2019). Typically, if the fibre treatment is carried out at high temperatures, the crystallinity degree increases, thus reducing the oxygen diffusion and making the fibres intrinsically safer. Uncontrolled treatments can however cause the formation of defects in the material with an increase in the amorphous fraction with an unfavourable effect in terms of safety (Kim et al., 2019; Okuno et al., 1992). Also in this case, the effects of the treatments on the fibres must be evaluated *a priori* to be able to design appropriate safety measures.

6. Conclusions

The size of nylon 6.6 fibres, considered in terms of equivalent diameter, is the main feature to be considered in the flammability and explosibility risk. Fibres with smaller equivalent diameter can be easily dispersed thus driving more easily the formation of a flammable cloud. In addition, smaller samples have a faster thermal degradation as observed both in inert and oxidative atmosphere. The higher reactivity exhibited in the thermal tests was confirmed in the flammability tests as shown by the measured values of the minimum ignition energy. Dimensionless analysis allowed the evaluation of the step controlling the fibre reaction paths. It was found that both the homogeneous and the heterogeneous reactive paths play a significant role in affecting the reactivity of the samples. In the homogeneous path, the pyrolysis controls flame propagation path while the heterogeneous combustion path is controlled by the intrinsic kinetic and then mainly affected by the specific surface area. All these results suggest that to reduce reactivity/flammability, the key phenomena affecting the reaction progress must be identified and quantified. Moreover, all the treatments (e.g., superficial ones) that can influence and modify these key parameters should be examined in order to evaluate the feasibility and if possible try to apply procedures to obtain an intrinsically safe material.

Author statement

Maria Portarapillo: Conceptualization; Methodology; Investigation; Validation; Visualization; Writing – original draft. **Enrico Danzi:** Methodology, Writing - Review & Editing. **Gianluca Guida:** Investigation. **Giuseppina Luciani:** Methodology, Writing - Review & Editing. **Luca Marmo:** Methodology, Writing - Review & Editing. **Roberto Sanchirico:** Methodology, Writing - Review & Editing. **Almerinda Di Benedetto:** Conceptualization; Methodology; Visualization; Writing – original draft; Supervision.

Declaration of competing interest

The authors declare that they have no known competing financial interests or personal relationships that could have appeared to influence the work reported in this paper.

Acknowledgements

Author acknowledge Mr. Andrea Bizzarro for his excellent technical support and Mr. Luciano Cortese for SEM analysis.

Appendix A. Supplementary data

Supplementary data to this article can be found online at https://doi.org/10.1016/j.jlp.2022.104815.

References

Amyotte, P., Domaratzki, R., Lindsay, M., MacDonald, D., 2011. Moderation of explosion likelihood and consequences of non-traditional dusts. Inst. Chem. Eng. Symp. Ser. 148–154.

Amyotte, P., Khan, F., Boilard, S., Iarossi, I., Cloney, C., Dastidar, A., Eckhoff, R., Marmo, L., Ripley, R., 2012. Explosibility of nontraditional dusts: experimental and modeling challenges. Inst. Chem. Eng. Symp. Ser. 83–90.

ASTM D7582 - 15, 2015. Standard Test Methods for Proximate Analysis of Coal and Coke by Macro Thermogravimetric Analysis. ASTM Int. West, Conshohocken, PA.

ASTM E1226-19, 2019. Standard Test Method for Explosibility of Dust Clouds. ASTM Int. West Conshohocken, PA 1–15. https://doi.org/10.1520/E1226-19.

ASTM International, 2003. Standard Test Method for Minimum Ignition Energy of a Dust Cloud in Air, pp. 1–11.

Bragg, W.H., Bragg, W.L., 1913. The reflexion of X-rays by crystals. Proc. Roy. Soc. Lond. A. 88, 428–438. https://doi.org/10.1098/rspa.1913.0040.

Centrella, L., Portarapillo, M., Luciani, G., Sanchirico, R., Di Benedetto, A., 2020. Synergistic behavior of flammable dust mixtures: a novel classification. J. Hazard Mater. 397, 122784 https://doi.org/10.1016/j.jhazmat.2020.122784.

Debye, P., Scherrer, P., 1916. Interference of irregularly oriented partcles in x-rays. Phys 17, 277–283.

Di Benedetto, A., Russo, P., 2007. Thermo-kinetic modelling of dust explosions. J. Loss Prev. Process. Ind. 20, 303–309. https://doi.org/10.1016/j.jlp.2007.04.001.

Di Benedetto, A., Russo, P., Amyotte, P., Marchand, N., 2010. Modelling the effect of particle size on dust explosions. Chem. Eng. Sci. 65, 772–779. https://doi.org/10.1016/j.ces.2009.09.029.

Diaz-Alejo, L.A., Menchaca-Campos, E.C., Chavarin, J.U., Sosa-Fonseca, R., Garcia-Sanchez, M.A., 2013. Effects of the addition of ortho- and para-N[H.sub.2] substituted tetraphenylporphyrins on the structure of Nylon 66. Int. J. Polym. Sci 2013, 1–14.

Hornsby, P.R., Wang, J., Rothon, R., Jackson, G., Wilkinson, G., Cossick, K., 1996. Thermal decomposition behaviour of polyamide fire-retardant compositions containing magnesium hydroxide filler. Polym. Degrad. Stabil. 51, 235–249. https://doi.org/10.1016/0141-3910(95)00181-6.

Hossain, M.N., Amyotte, P.R., Khan, F.I., Abuswer, M.A., Skjold, T., Morrison, L.S., 2013. Dust explosion quantitative risk management for nontraditional dusts. Chem. Eng. Trans. 31, 115–120. https://doi.org/10.3303/CET1331020.

Iarossi, I., Amyotte, P.R., Khan, F.I., Marmo, L., Dastidar, A.G., Eckhoff, R.K., 2013. Explosibility of polyamide and polyester fibers. J. Loss Prev. Process. Ind. 26, 1627–1633. https://doi.org/10.1016/j.jlp.2013.07.015.

Kim, K.W., Jeong, J.S., An, K.H., Kim, B.J., 2019. A study on the microstructural changes and mechanical behaviors of carbon fibers induced by optimized electrochemical etching. Compos. B Eng. 165, 764–771. https://doi.org/10.1016/j.compositesb.2019.02.055.

Krishna Prasad, G., Periyasamy, S., Chattopadhyay, S.K., Raja, A.S.M., Rajkumar, K., Jagadale, S., 2017. Surface modification of nylon fabric and its optimization for improved adhesion in rubber composites. J. Text. Inst. 108, 1001–1009. https://doi.org/10.1080/00405000.2016.1209826.

Krump, H., Šimor, M., Hudec, I., Jaššo, M., Luyt, A.S., 2005. Adhesion strength study between plasma treated polyester fibres and a rubber matrix. Appl. Surf. Sci. 240, 268–274. https://doi.org/10.1016/j.apsusc.2004.06.109.

Liu, H., Wang, C., Zhang, J., Zhao, W., Fan, M., 2020. Pyrolysis kinetics and thermodynamics of typical plastic waste. Energy Fuel. 34, 2385–2390. https://doi.org/10.1021/acs.energyfuels.9b04152.

Maher, R.R., Wardman, R.H., 2015. The Chemistry of Textile Fibres, second ed. Royal Society of Chemistry, UK.

Marmo, L., Cavallero, D., 2008. Minimum ignition energy of nylon fibres. J. Loss Prev. Process. Ind. 21, 512–517. https://doi.org/10.1016/j.jlp.2008.04.003.

Marmo, L., Sanchirico, R., Di Benedetto, A., Di Sarli, V., Riccio, D., Danzi, E., 2018. Study of the explosible properties of textile dusts. J. Loss Prev. Process. Ind. 54, 110–122. https://doi.org/10.1016/j.jlp.2018.03.003.

Michaels, A.S., Bixler, H.J., 1961. Flow of gases through polyethylene. J. Polym. Sci. 50, 413–439. https://doi.org/10.1002/pol.1961.1205015412.

Nabatame, T., Yasuda, T., Nishizawa, M., Ikeda, M., Horikawa, T., Toriumi, A., 2003. Comparative studies on oxygen diffusion coefficients for amorphous and γ-al2o3 films using 18O isotope. Jpn. J. Appl. Phys., Part 1 Regul. Pap. Short Notes Rev. Pap. 42, 7205–7208. https://doi.org/10.1143/jjap.42.7205.

Okuno, T., Yasuda, T., Yasuda, H., 1992. Effect of crystallinity of PET and nylon 66 fibers on plasma etching and dyeability characteristics. Textil. Res. J. 62, 474–480. https://doi.org/10.1177/004051759206200807.

Portarapillo, M., Luciani, G., Sanchirico, R., Di Benedetto, A., 2020. Ignition mechanism of flammable dust and dust mixtures: an insight through thermogravimetric/differential scanning calorimetry analysis. AIChE J. 66 https://doi.org/10.1002/aic.16256.

Professional Plastics. Thermal properties of plastic materials. n.d [WWW Document]. URL. https://www.professionalplastics.com/professionalplastics/ThermalPropertiesofPlasticMaterials.pdf.

Ranz, W.E., Marshall Jr., W.R., 1952. Evaporation from drops. Chem. Eng. Prog. 48, 173–180 (part i) 141–146 and (part ii).

Rowe, P.N., Claxton, K.T., Lewis, J.B., 1965. Heat and mass transfer from a single sphere in an extensive flowing fluid. Trans. Inst. Chem. Eng. 43, T14–T31.

Russo, P., Amyotte, P.R., Khan, F.I., Di Benedetto, A., 2013. Modelling of the effect of size on flocculent dust explosions. J. Loss Prev. Process. Ind. 26, 1634–1638. https://doi.org/10.1016/j.jlp.2013.07.012.

Schneider, C.A., Rasband, W.S., Eliceiri, K.W., 2012. NIH Image to ImageJ: 25 years of image analysis. Nat. Methods 9, 671–675. https://doi.org/10.1038/nmeth.2089.

2021. https://sewport.com/fabrics-directory/nylon-fabric [WWW Document].

Sirane Group, 2021. Product spotlight: nylon is great for oven-ready packaging AND food service [WWW Document]. URL. https://www.sirane.com.

Starkweather, H.W., Zoller, P., Jones, G.A., 1984. Heat of fusion of 66 nylon. J. Polym. Sci. 2 Polym. Phys. 22, 1615–1621. https://doi.org/10.1002/pol.1984.180220905.

Tricor Flexible Packaging Inc., 2021. How Nylon film is made [WWW Document]. https://www.tri-cor.com/.

Worsfold, S.M., Amyotte, P.R., Khan, F.I., Dastidar, A.G., Eckhoff, R.K., 2012. Review of the explosibility of nontraditional dusts. Ind. Eng. Chem. Res. 51, 7651–7655. https://doi.org/10.1021/ie201614b.

Xia, H., Peng, J., Zhang, L., 2015. Preparation of high surface area activated carbon from Eupatorium adenophorum using K2CO3 activation by microwave heating. Green Process. Synth. 4, 299–305. https://doi.org/10.1515/gps-2015-0025.

Zhao, L.J., Sun, Q., 2013. Calculations of effectiveness factors and the criteria of mass transfer effect for hightemperature methanation (HTM) catalyst. Int. J. Low Carbon Technol. 10, 288–293. https://doi.org/10.1093/ijlct/ctu005.

Zille, A., Oliveira, F.R., Souto, P.A.P., 2015. Plasma treatment in textile industry. Plasma Process Polym 12, 98–131. https://doi.org/10.1002/ppap.201400052.